Volume phase holographic grating performance on the VIRUS-P instrument

Joshua J. Adams[a], Gary J. Hill[a,b], and Phillip J. MacQueen[a,b]

[a]University of Texas at Austin, Department of Astronomy, 1 University Station, C1400, Austin, USA;
[b]McDonald Observatory, 1 University Station, C1402, Austin, USA

ABSTRACT

The Visible Integral-field Replicable Unit Spectrograph Prototype (VIRUS-P) has been in operation on the Harlan J Smith 2.7m Telescope at McDonald Observatory since October of 2006. The prototype was created to test the design and science capabilities of the full VIRUS instrument, wherein 150 copies of the spectrograph will be installed on the Hobby Eberly Telescope (HET). We here discuss the specialized test bench built to assess the blue optimized Volume Phase Holographic (VPH) grating performance. We also give lab and on-telescope efficiency measurements for three such gratings in the wavelength range 3400-6800Å. Two sources of stray light relevant to most spectrograph designs are also discussed.

Keywords: astronomical spectrographs, volume phase holographic gratings, integral field, dark energy, HETDEX, VIRUS

1. INTRODUCTION

HETDEX will discover spectroscopically 800,000 new Lyman-alpha Emitting galaxies (LAEs) for use as probes of baryonic acoustic oscillation in the early universe which can be used to measure the strength of dark energy and its possible evolution in a currently unmeasured epoch.[1] This 120 night survey will use 150 modified copies of the exising VIRUS-P instrument placed on the 9.2m HET. The overall instrument design is described in Ref. 2, the camera design and performance in Ref. 3, and tests of the fiber optic bundles in Ref. 4. We here detail tests and optimizations that have been performed on the VPH gratings that act as the dispersion elements in these spectrographs at transmission order m=1. Our results push the technology to high efficiency at bluer wavelengths than has been previously published as we need to operate to 3400Å. Besides the test results, we present details of the automated test bench we have created for repeatable and speedy measurements of the large quantity of gratings that HETDEX will eventually require. A test of more limited on-telescope performance verifies our test bench results. We also discuss two observed stray light paths that involve the grating. One is the Littrow reflection that is already known, but the second is a higher dispersion, redder pattern that is new to the literature.

2. GRATINGS

We have acquired three VPH gratings for potential use in the VIRUS-P instrument. All three are sandwiched between fused silica plates of glass yielding a total size of 140x140x17mm^3. The optically active surface for our purposes is a centered circle of diameter 130mm. All three gratings share a modulation frequency of 831 lines/mm and have unslanted fringes. We know neither the dichromated gelatin layer thicknesses nor the amplitudes of refractive index modulation, so we cannot estimate efficiencies with the Kogelnik approximation.[5] The two gratings provided by Wasatch photonics are a holographic master and copy ideally sharing all properties we will hereafter call H1 and C1. The copy is made by a method unknown to us, but which promises lower unit cost as desirable for the multiplexing nature of the VIRUS design. The third grating was provided by Kaiser Optical Systems Inc. (KOSI). Rigorous coupled wave analysis[6] (RCWA) was performed by KOSI for their design as shown in Fig. 1.

Further author information: (Send correspondence to J.J.A.)

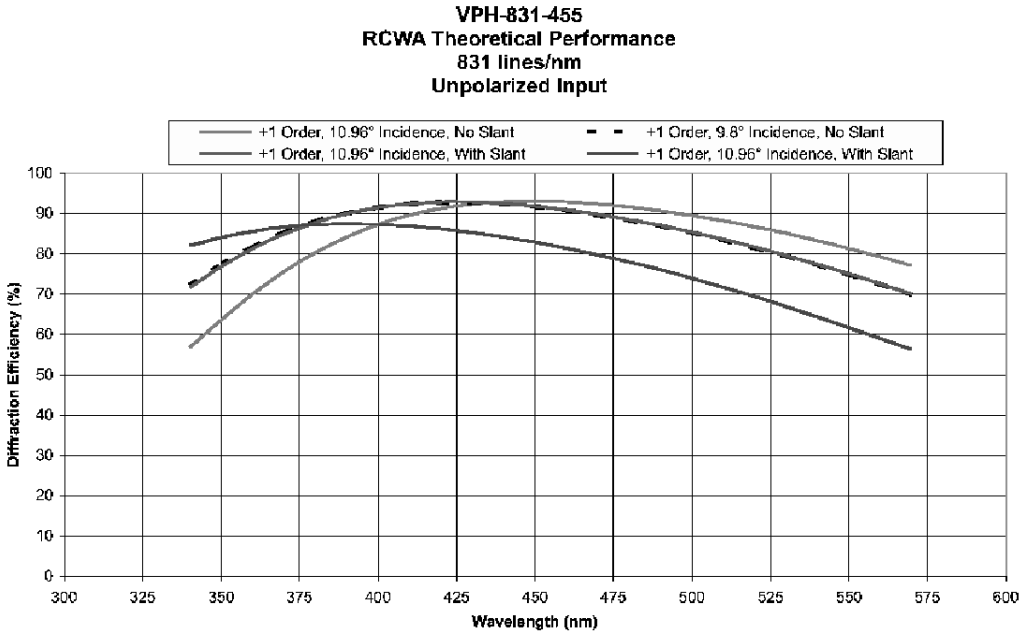

Figure 1. RCWA performed by KOSI for their grating.

3. TEST BENCH

3.1 Components

We have built an automated optical test bench to measure the wavelength dependent efficiency of diffraction gratings under general conditions. The very simple design is inspired by the tunable spectrograph concept sketched in Ref. 7. Figure 2 shows our design. A commercial monochromator is coupled to a fiber optics bundle. A filter wheel lies just prior to the output slit with a set of filters to block out second order light for any configuration. The monochromator can use a 100W quartz tungsten halogen (QTH) or 30W deuterium lamp as input. The deuterium lamp gives us access to the 3400-4500Å UV range which is crucial to the survey science. We use large, matched input and output slits of size 0.76mm in our monochromator to improve signal strength in the bench tests. This translates at 5000Å to a bandpass of 21Å in our measurements. The monochromatic light leaves the fiber bundle and becomes collimated by a 50mm diameter fused silica singlet. An adjustable iris then cuts down the beam to the desired size. All measurements presented here used a 19mm diameter collimated beam. The collimated beam next transmits through our grating. The grating rests in a mount whose back surface has been aligned as normal to the input beam to within 0.1°. This grating mount sits on a stepper motor rotation stage of 0.01° accuracy. The beam travels from the grating to a focusing lens identical to the collimating lens. This lens brings the image to a focus in the middle of a 10mm diameter Fabry, or pupil, fused silica lens. The Fabry lens improves measurement stability by imaging the exit pupil of the fiber bundle onto the final component, a silicon single element 5mm diameter photodiode. The spot delivered to the photodiode is of size 0.56mm across the monochromator bandpass per a ray tracing model and safely an order of magnitude smaller than the photodiode surface. Laboratory tests verify this by showing that the measured efficiency is constant to within 1% until the output angle at measurement, β, deviates from that demanded by the simple grating equation by more than $\pm 0.5°$. All elements acting after the grating are on a second stepper motor rotation stage which rotates with accuracy 0.001° around the same axis as the grating rotation stage. All operations,

J.J.A.: E-mail: jjadams@astro.as.utexas.edu.edu, Telephone: 1 512 471 3447
G.J.H.: E-mail: hill@astro.as.utexas.edu, Telephone: 1 512 471 1477
P.J.M.: E-mail: pjm@astro.as.utexas.edu, Telephone: 1 512 471 1470

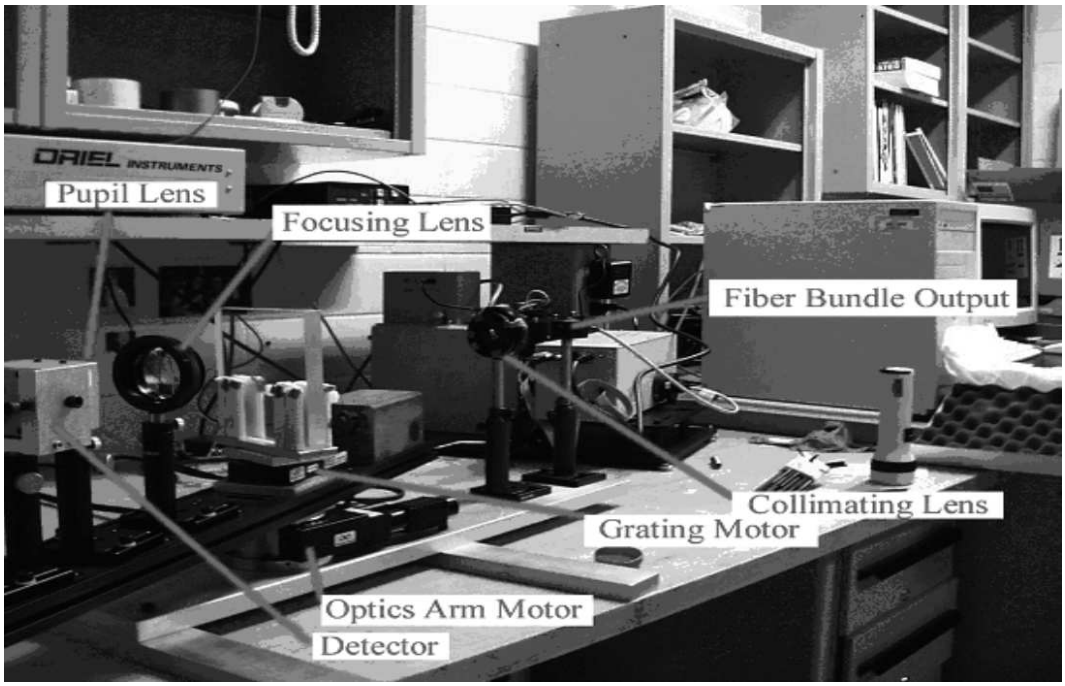

Figure 2. The grating test bench optical layout. The setup has been removed from its light box for display.

from monochromator control to motor movements to detector readout, are controlled through a computer and custom written software. This simple design allows us to measure diffraction grating efficiency as a function of wavelength, input angle, and diffraction order. We are also capable of scanning through angles outside of Bragg diffraction for scattered or reflected light.

3.2 Operating Procedure

We begin a measurement with both α and β set to 0° and the mount absent a grating. We step through all wavelengths of interest with the monochromator. Each measurement consists of a light reading with the light path open followed by a dark reading with a shutter in the monochromator closed. The subtraction of these two removes any bias and background. This step establishes the amount of light being delivered through the system without the grating. The diffraction grating is then inserted, and measurements are taken through all wavelengths and angles of interest. The ratio of the dark subtracted grating measurement to the dark subtracted normalization measurement gives the grating efficiency. At the end of all scans, the normalization measurements are again checked to evaluate lamp stability. In all measurements presented, the post-measurement normalization intensity was within 2% or better of the pre-measurement normalization itensity at all wavelength.

4. RESULTS

4.1 Efficiency with Input Angle

The wavelength of peak efficiency at a particular α can be easily estimated through the Bragg condition. However, the efficiency envelope at other wavelengths has no easy estimation. This envelope is often asymmetric with the dropoff less severe at wavelengths redward of the Bragg condition. RCWA can make these predictions, but imperfections in the manufacturing process can further degrade performance. For our instrument, we desire high efficiency in the survey wavelength range of 3400-5700Å, with emphasis on the bluer region. Our prototype spectrograph is tunable in α, so off-design performance at higher wavelengths is of interest for our side science applications. However, this performance does not drive our design. Figures 3, 4, and 5 show the measured performance through a variety of α's. We are still falling below RCWA predictions, so we believe further development work may improve final grating performance. Interestingly, the RCWA curve at $\alpha = 9.8°$ best

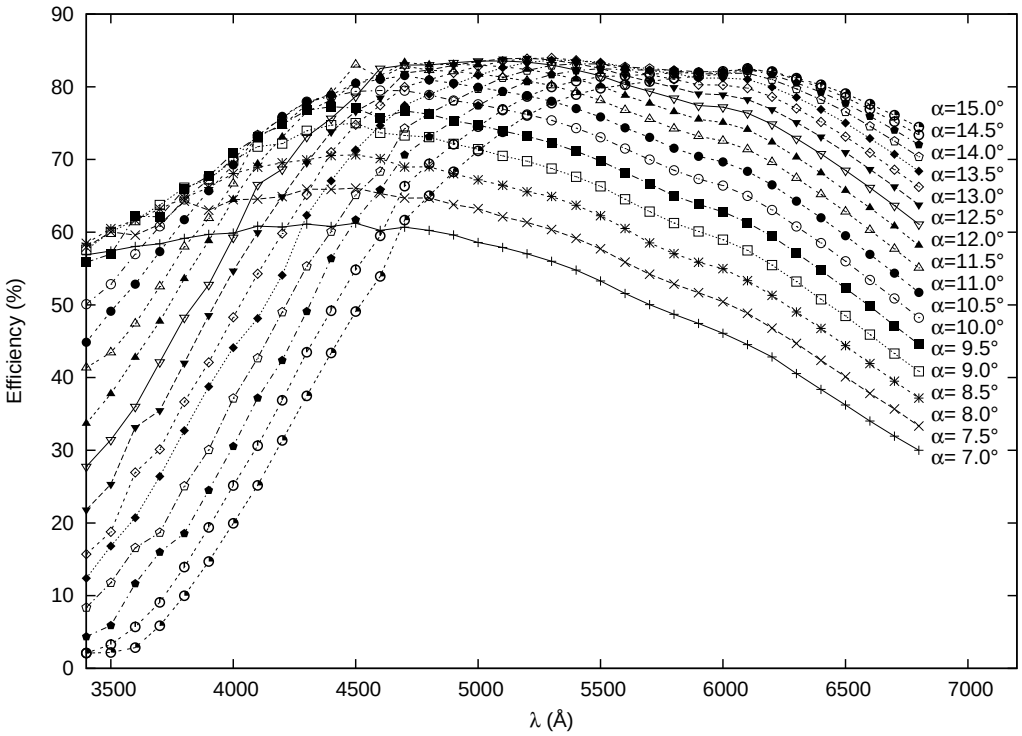

Figure 3. The laboratory measurement of the KOSI grating first order efficiency as a function of input angle and wavelength.

matches the data measured for the $\alpha = 9.0°$ curve. This is well outside our possible alignment error in α, and we cannot explain this discrepancy. The Wasatch H1 grating reaches a roughly equal peak efficiency as the KOSI grating, but the efficiency envelope dropoff is stronger. Notably at 3400Å, the extra loss is 10%. The copy has extra loss over the master, although this effect is not severe at the bluest wavelengths. The extra loss in the copy is 10% at the region of peak efficiencies near 4500Å.

4.2 Efficiency with Diffraction Order

We can investigate the types of efficiency loss by looking at diffraction orders other than m=1. This is shown in Fig. 6. At the bluest wavelengths, the main thief from m=1 is the m=2 order. At off-design redder wavelengths, the main thief is the m=0 order. There is obvious correlation between a rising strength in the m=0 or m=2 orders and a drop in the m=1 order for all gratings. This serves as validation for our measurements.

4.3 Laboratory Verification

A scan outside of the usual, simple grating equation will reveal two important features: any non-ideal scattered light being caused by the grating and an input light source that is not properly monochromatic. We give such scans at two wavelengths in Figs. 7 and 8. We have zoomed in our plot to low signal levels. The m=0,1,and 2 orders are where expected and often rise off the charts. Figure 7 shows a curious feature near $\beta = -23°$. Here, for both gratings the intensity unexpectedly rises. We have investigated this with cutoff filters and found that this is not a scattered light component. Instead, this is an imperfection in our commercial monochromator. The very red QTH source produces undesired emission through the monochromator around 6800Å. This will affect our measurement by causing an overestimate in the normalization reading. For the case given, the error contributes a fraction of a percent to the final measurement which is below our interest. However, this error becomes more severe for bluer wavelengths as the strength of the source intrinsically becomes dimmer. It is for this reason that we have used the deuterium lamp for all measurements between 3400-4600Åand the QTH lamp only for redder wavelengths. A β scan for the deuterium source in Fig. 8 does not show a similar bump as expected for the

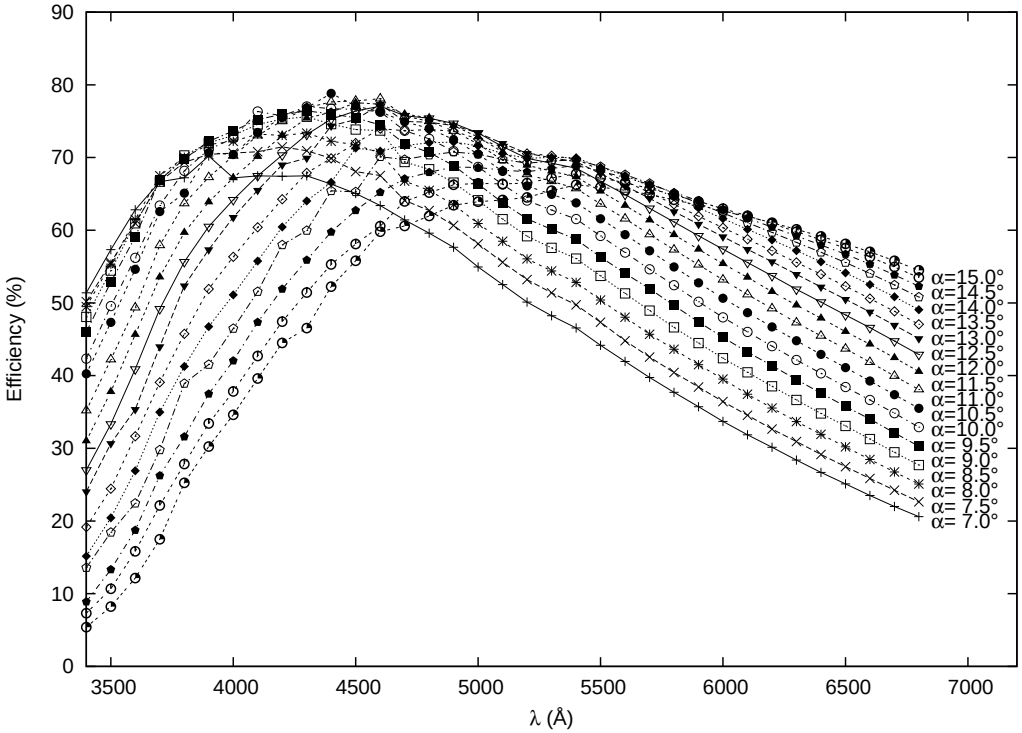

Figure 4. The laboratory measurement of the H1 first order efficiency as a function of input angle and wavelength.

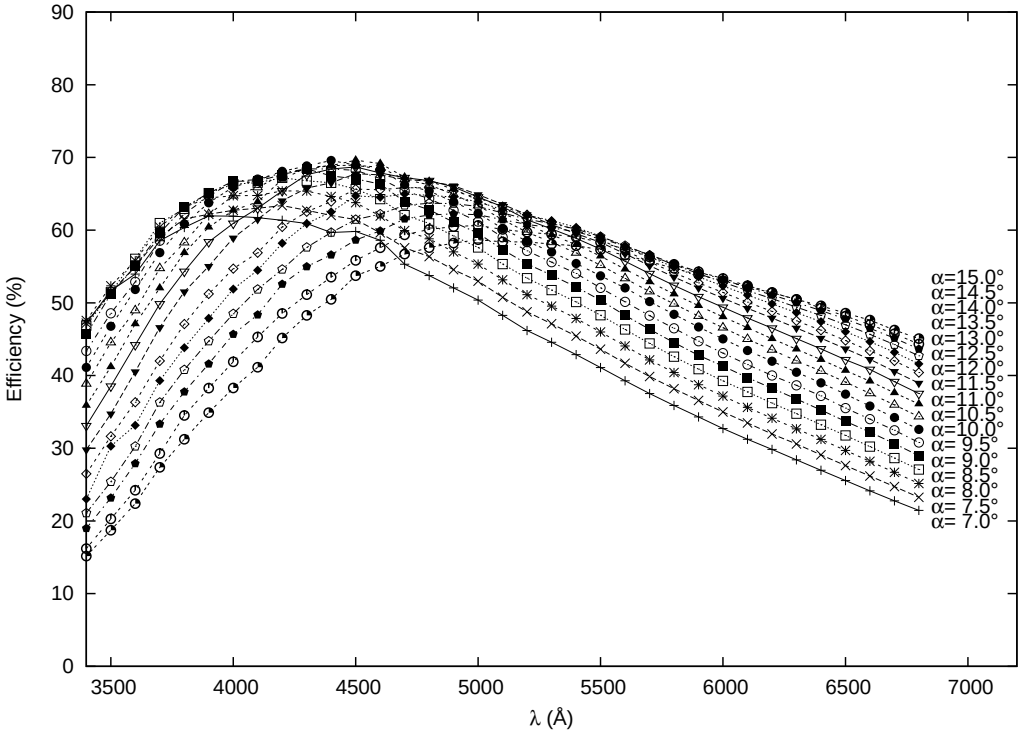

Figure 5. The laboratory measurement of the C1 first order efficiency as a function of input angle and wavelength.

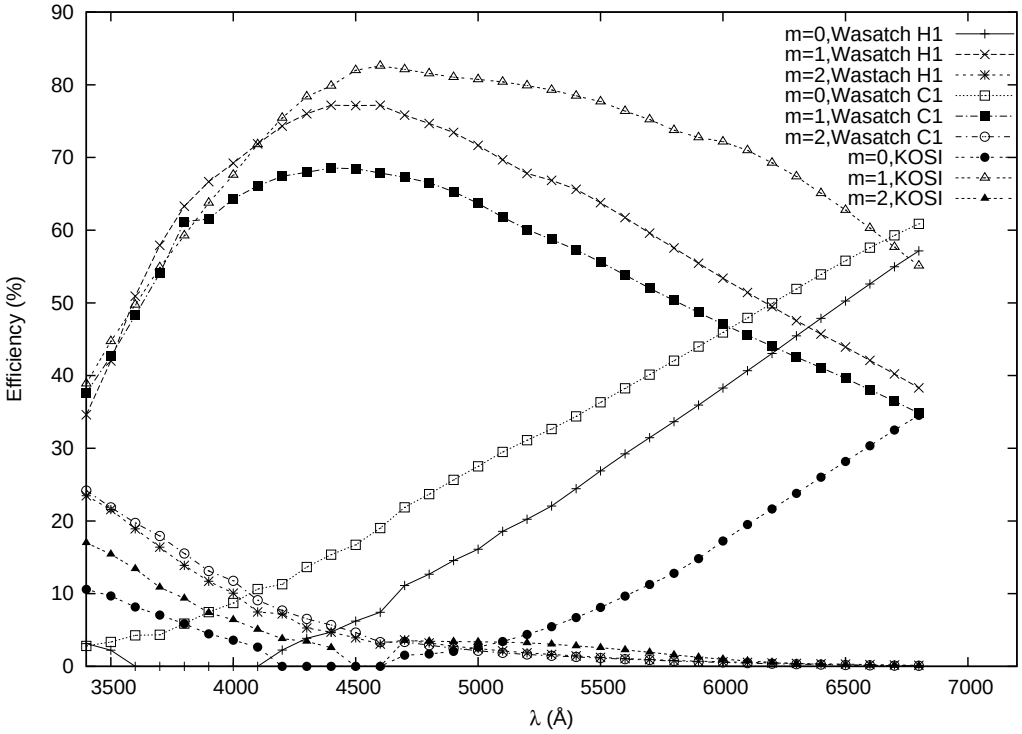

Figure 6. The laboratory measurement of diffraction orders 0,1,and 2 for $\alpha = 10.5°$.

bluer intrinsic deuterium spectrum. The deuterium scan does show increased measurement noise as the signal is much weaker at these wavelengths, but this error is 2% or lower in all cases.

4.4 On Telescope Verification

Independently from our test bench, we have measured the efficiency of the KOSI and H1 gratings on the 2.7m McDonald Observatory telescope with the full VIRUS-P instrument. We cannot measure an absolute grating efficiency in this case, but the ratio of the two measurements can be used to validate our lab data. Figure 9 shows the result. On telescope, we used a QTH lamp against the dome wall. This is a very red source, so we cannot directly measure by this method the efficiency of the bluest wavelengths due to lack of flux. However, in the wavelength regions that overlap, we find excellent agreement between the on-telescope and in-lab ratios.

5. STRAY LIGHT

5.1 Narcissus

During the VIRUS-P pilot survey, we have observed two types of stray light that were not initially expected in the design. When taking data on bright standard stars, we found an apparent emission line displaced from the standard star by eight fibers. Through moving the telescope position, we found that this putative emission line did not stay in a fixed location on the sky, but instead stayed a fixed distance in detector space from the bright, standard star spectra. We identify this as "narcissus" discussed in Ref. 8 with a slight out-of-plane angle between optical surfaces giving the eight fiber offset. Narcissus occurs in a spectrograph when light traveling the designed path reflects from the CCD, diffracts again through the dispersion element, and returns to the CCD. In the specific case where the dispersion orders of each pass are identical, the stray light is called a "Littrow ghost".[9] In this case, which we observe, there is no dispersion in the final ghost. Although we are not usually operating with the Littrow wavelength centered in our bandpass, the wavelength is still within our bandpass so the Littrow ghost gets imaged. The stray light will exit the grating at the input angle, α. The measured

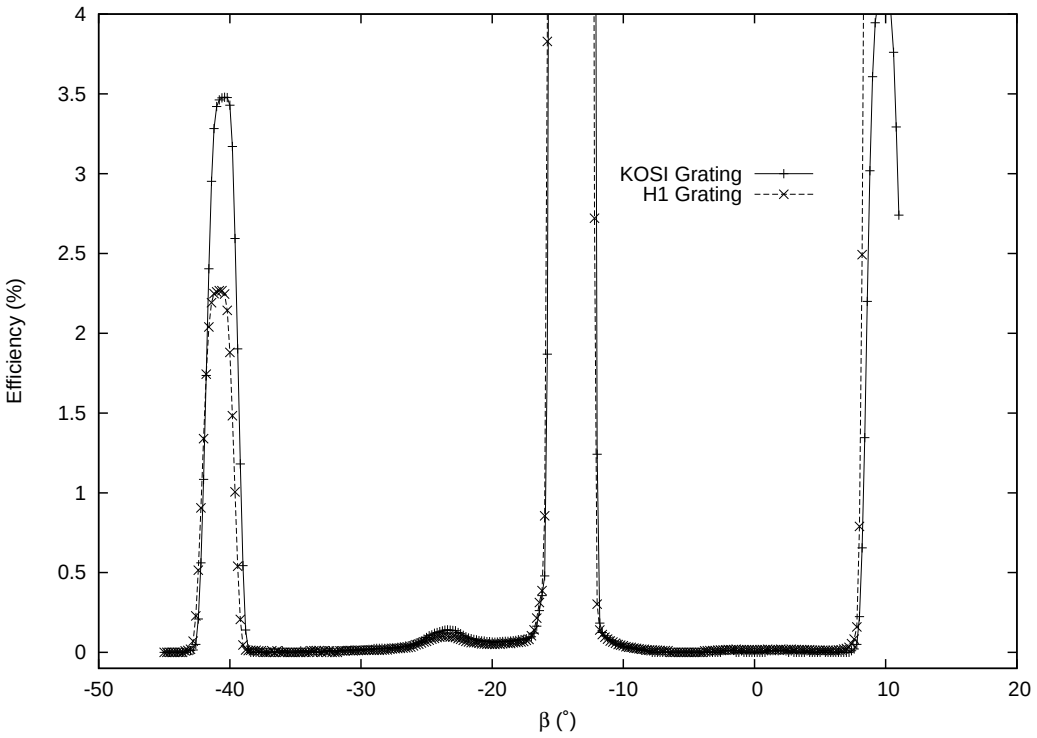

Figure 7. A scan across output angle to search for scattered or polychromatic light with the QTH source at $\alpha = 10^\circ$ and λ=5000Å.

Littrow ghost in VIRUS-P is within 0.1° of the α we measured through an inclinometer which has a comparable measurement resolution. If not accounted for, this could be a dangerous contaminant to our science goals. For the detection of LAEs, our only signal is from a solitary emission line that looks very similar to this stray light. With the Littrow ghost known, however, we can exclude the detector position around the rare, bright objects in our survey area and avoid sample contamination.

5.2 High Dispersion, Red Contamination

A second source of stray light becomes obvious when we take neon arc lamp frames. Neon has a large number of bright emission lines that should lie redward of our recorded data. The pattern of these red lines is superimposed on the proper neon spectrum, but with double dispersion and double the expected curvature with γ. We installed better baffling around the camera window which cut down but did not eliminate this feature. The stray light path we have found that can cause this behavior is as follows: first order transmissive diffraction, reflection from the camera window, reflection from the grating (can be either reflection from the front surface of the grating's glass, zeroth order reflective diffraction, or zeroth order transmissive diffraction followed by reflection from the rear surface of the grating's glass and then another zeroth order transmissive diffraction), another reflection from the camera window, and finally another first order diffraction of the light (can be either a first order reflective diffraction or a zeroth order transmissive diffraction followed by a reflection from the rear glass surface and then a first order transmissive diffraction). Fig. 10 shows this stray light path that images red light which normally would strike baffling or the inner wall of the camera chamber. For a simplified, analytic model we can ignore the slight curvature in the camera window's front surface and the wavelength dependent refractive index of the fused silica window and treat all the reflections as from flat surfaces. Doing this, we can derive Eq. 1 where α is the input angle for the light entering the grating, β_c is the angle between the normal of the camera window and the normal of the grating, λ_s is the stray light wavelength, λ_p is the proper wavelength of light that should be imaged on the detector position where the stray light of λ_s is appearing, and σ is the spacing between fringes in

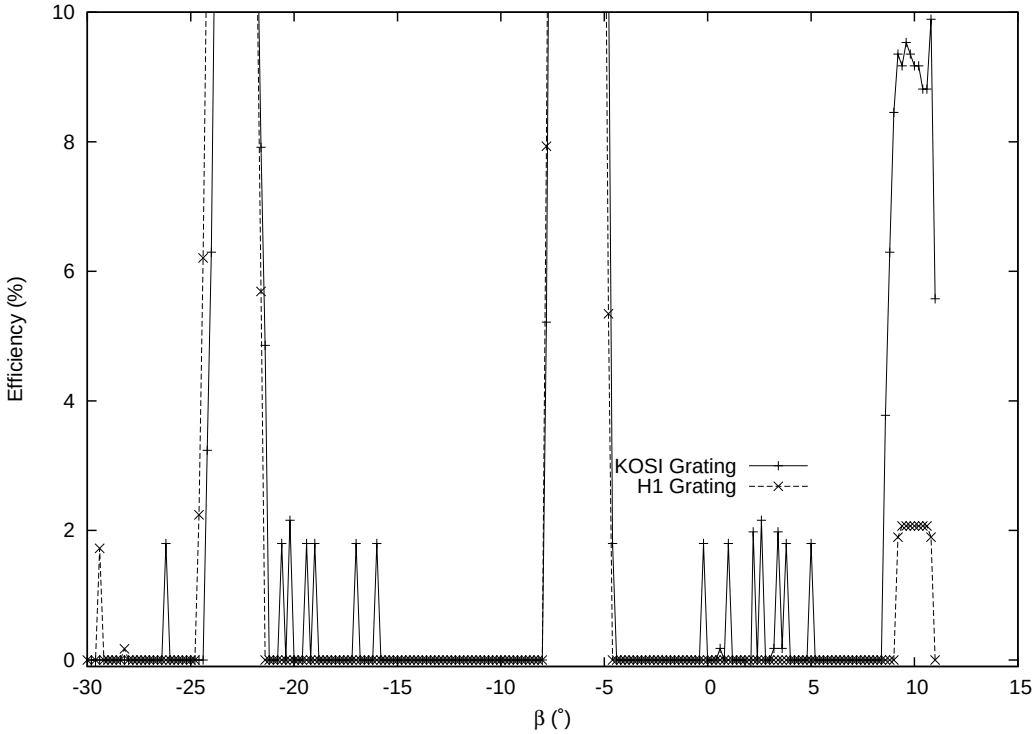

Figure 8. A scan across output angle to search for scattered or polychromatic light with the deuterium source at $\alpha = 10^\circ$ and λ=3400Å.

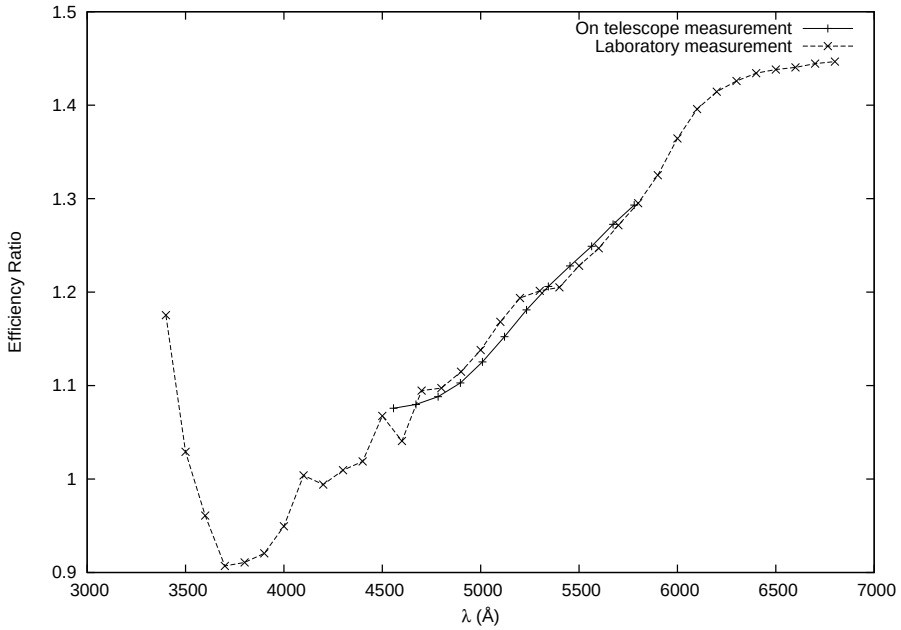

Figure 9. The ratio of first order efficiency between the KOSI and H1 gratings as measured on-telescope and in-lab at $\alpha = 10.5^\circ$.

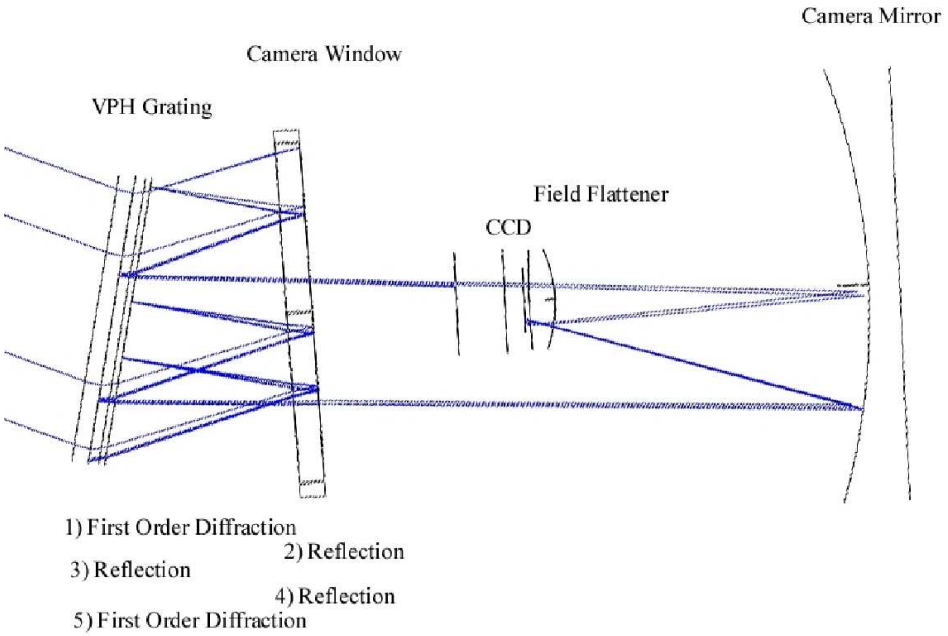

Figure 10. The stray light path that images red, high dispersion light.

the same unit as all the wavelengths.

$$\frac{\lambda_p}{\sigma} = \frac{\lambda_s}{\sigma} + \sin\alpha + (\frac{\lambda_s}{\sigma} - \sin\alpha)\cos(4\beta_c) - \sqrt{1 - (\frac{\lambda_s}{\sigma} - \sin\alpha)^2}\sin(4\beta_c) \quad (1)$$

The wavelength solution from readout data informs us very well of the angle between the camera mirror and the grating normal, which we can also adjust. Assuming the camera window has the exact same axis as the camera mirror gives a poor fit to our observations of the stray, red light. However, we installed the camera and adjusted the camera mirror for optimal image quality which may have tilted the angle between the camera mirror and the normal to the camera window. If we allow an offset of 1.5° between these surfaces, we find the model matches in Table 5.2. We estimate the strength of this stray light from the observed arc lamps lines in a similar neon lamp on the Low Resolution Spectrograph (LRS) on the HET. Roughly assuming a similar relative instrument response across wavelength between the LRS and VIRUS-P, we measure the attenuation factors for this light again in Table 5.2 with our current best baffling around the camera window. These measurements are high compared to our expectation for three reflections of 10^{-6}. However, it may be that the anti-reflection coatings are not operating at these wavelengths so far off design. This discrepancy remains as mild evidence against the stray light path we have given. Now that we have found this source of stray light, we can create further baffling to attenuate the stray light without affecting the desired signal. In particular, the rear side of the VPH grating has a surrounding surface of glass that is currently unbaffled. This surface in no way contributes to the desired optical path, but does give red light more area in the stray light's second reflection. This improvement will be important scientifically as currently the stray light from the night sky line [OI]λ6300 with higher curvature with γ causes a minor residual in our background subtraction and interferes with automatic LAE detection algorithms.

6. CONCLUSION

The tunable nature and the broad efficiency envelopes that VPH gratings display over traditional ruled gratings are essential to reaching the low flux limits required by our science. We find that the performance results that have been documented at wavelengths in the middle of the visible spectrum can be pushed down to blue and

Table 1. The observed red stray light compared to our stray light model. The match is convincing considering the simplifications we made in the reflections from the camera window and that different line curvatures between the proper and stray light spectra make this measurement vary over the chip at the level of the wavelength residual.

α	β_c	λ_s	Model λ_p	Measured λ_p	Attenuation Factor
10.6	10.4	6438.5	4330.6	4377.7	2E-3
11.0	15.1	8377.6	4656.2	4689.6	3E-2
11.0	15.1	8495.4	4893.0	4767.5	4E-2
11.0	15.1	8654.4	5215.1	5196.0	4E-2
11.0	15.1	8780.6	5472.9	5401.5	4E-2

UV wavelengths successfully without an obvious need for slanted fringes, but that RCWA predictions are not yet being achieved. We expect further iterations of design and sample manufacturing from our vendors, but counting the current results as the worst case for the final design gives us first order efficiency of 60% at 3400Å and 85% at 5000Å. Our test bench, with its computer controlled, automated operation, will be essential for the large quantity characterization that will be required for HETDEX.

ACKNOWLEDGMENTS

We thank Gerald Heidt at Wasatch Photonics and Jim Arns at KOSI for their products and ongoing measurements. We thank Jim for providing the RCWA plot shown above. JJA acknowledges funding from a National Science Foundation Graduate Research Fellowship.

REFERENCES

[1] Hill, G. J., Gebhardt, K., Komatsu, E., Drory, N., MacQueen, P. J., Adams, J. J., Blanc, G. A., Koehler, R., Rafal, M., Roth, M. M., Kelz, A., Gronwall, C., Ciardullo, R., and Schneider, D. P., "The Hobby-Eberly Telescope Dark Energy Experiment (HETDEX): Description and Early Pilot Survey Results," in [*Panoramic Views of the Universe*], *ASP conference series* (2008).

[2] MacQueen, P. J., Hill, G. J., Smith, M. P., Tufts, J. R., Barnes, S. I., Roth, M. M., Kelz, A., Adams, J. J., Blanc, G., Murphy, J. D., Altmann, W., Wesley, G. L., Segura, P. R., Good, J. M., Goertz, J. A., Edmonston, R. D., and Wilkinson, C. P., "Design, construction, and performance of VIRUS-P: the prototype of a highly replicated integral field spectrograph for the HET," in [*Astronomical Telescopes and Instrumentation*], *Proc. SPIE* **7014-257** (2008).

[3] Tufts, J. R., MacQueen, P. J., Smith, M. P., Segura, P. R., Hill, G. J., and Edmonston, R. D., "VIRUS-P: camera design and performance," in [*Astronomical Telescopes and Instrumentation*], *Proc. SPIE* **7021-10** (2008).

[4] Murphy, J., Palunas, P., Grupp, F., MacQueen, P. J., Hill, G. J., Kelz, A., and Roth, M., "Focal ratio degradation and transmission in VIRUS-P optical fibers," in [*Astronomical Telescopes and Instrumentation*], *Proc. SPIE* **7018-104** (2008).

[5] Kogelnik, H., "Coupled-wave theory for thick hologram gratings," in [*Bell System Tech. J.*], **48**, 2909–2947 (1969).

[6] Gaylord, T. K. and Moharam, M. G., "Analysis and applications of optical diffraction by gratings," in [*Proc. IEEE*], **73**, 894–937 (1985).

[7] Barden, S. C., Arns, J. A., and Colburn, W. S., "Volume-phase holographic gratings and their potential for astronomical applications," in [*Optical Astronomical Instrumentation*], D'Odorico, S., ed., *Proc. SPIE* **3355**, 866–876 (July 1998).

[8] Tull, R. G., MacQueen, P. J., Sneden, C., and Lambert, D. L., "The high-resolution cross-dispersed echelle white-pupil spectrometer of the McDonald Observatory 2.7-m telescope," *PASP* **107**, 251–264 (Mar. 1995).

[9] Burgh, E. B., Bershady, M. A., Westfall, K. B., and Nordsieck, K. H., "Recombination Ghosts in Littrow Configuration: Implications for Spectrographs Using Volume Phase Holographic Gratings," *PASP* **119**, 1069–1082 (Sept. 2007).